

Modified graphene quantum dots targeting fibroblast growth factor receptor 2- photodynamic therapy for breast tumor

Youying Zhang ^{1, a}, Qi Xiang ^{2, b}

¹College of Pharmacy, Jinan University, Guangzhou 510632, P. R. China

²Institute of Biomedicine and Guangdong Provincial Key Laboratory of Bioengineering Medicine, Jinan University, Guangzhou 510632, P. R. China

^aqq329174818@163.com, ^btxiangqi@jnu.edu.cn

Abstract

It is well known that graphene quantum dots (GQDs) have ability to damage cells by means of inducing reactive oxygen species (ROS). However, GQDs are lack of tumor targeting. A short peptide named 8B13 is mimic peptide of FGF-8b. FGF-8b has ability to specifically bind fibroblast growth factor receptors (FGFRs) which over express in breast cancer cells. Therefore, the purpose of this research is to prepare a photodynamic agent based on GQDs and peptide 8B13 for tumor photodynamic therapy (PDT). Peptide 8B13-coupled chitosan covered polydopamine-modified GQDs nanohybrid (PDA-GQDs/CS-8B13) was prepared for tumor PDT. The particle size of PDA-GQDs/CS-8B13 was about 200 nm, and it took the shape of spheroidicity. Compared with GQDs, PDA-GQDs/CS-8B13 damaged more tumor cells after illumination. In comparison with MDA-MB-231 cells, the FGFRs high expressed breast cancer cells, SKBR-3 cells, took more PDA-GQDs/CS-8B13 and then induced more ROS. Owing to peptide 8B13, PDA-GQDs/CS-8B13 exhibited tumor targeting and stronger effect of PDT. The strategy that targeting ligands modified photodynamic agent has potential to improve curative effect.

Keywords

Graphene quantum dots, peptide 8B13, FGFR, breast cancer, photodynamic therapy.

1. Introduction

Graphene quantum dots (GQDs) are a kind of two-dimensional carbon nano-material with many excellent physicochemical properties, including biocompatibility, high photoluminescence, water-solubility, hypotoxicity, etc [1,2]. As a result, GQDs are explored in various field. Recent years, GQDs have been found that not only act as electron donor, but also electron acceptor. It means that GQDs have potential to be prooxidant and antioxidant [3]. When exposed to optical radiation, GQDs participate in a series of redox reaction to produce ROS, which causes oxidative stress. On the other hand, because of GQDs entering cytoplasm by the means of endocytosis, the majority of GQDs exist in intracytoplasmic vesicle [4]. The intracytoplasmic vesicles could combine with autophagic vacuoles that facilitates maturation for autophagic vacuoles. Autophagic vacuoles are supposed to renovate oxidatively damaged organelle and reduce cross-linked proteins [5]. However, high-level autophagy will induce apoptosis [6]. In other words, GQDs directly damage cells by means of ROS and indirectly damage cells by means of promoting autophagy. Therefore, GQDs have promising future in the field of photodynamic therapy.

Polydopamine (PDA) is one of research hotspot in recent years. PDA is prepared with dopamine as the raw material via facile reaction. Several polymerization pathways of PDA have been proposed [7]. However, the structure and polymerization mechanism of PDA are not clear completely. Owing to adhesive ability and biocompatibility, PDA has been widely explored in the field of biomaterial. The fluorescence intensity of GQDs is able to penetrate the solid tumor and tissue, which make it has potential to be used for fluorescence probe. It has been reported that PDA improved the fluorescence stability of GQDs [8]. Therefore, we prepared PDA-modified GQDs (PDA-GQDs).

FGFRs gene amplification, distal enhancer mutation and other gene mutations are likely to lead to FGFRs overexpression, which exert carcinogenesis and promote tumor growth [9]. Activation of FGFR signal path is universal phenomenon for tumorigenesis and tumor development. On the whole, compared with normal breast tissue, the protein expression level of FGFR1, FGFR2, FGFR3 and FGFR4 increases in breast cancer tissue [10,11]. For example, Sun *et al.* reported that they demonstrated high cytoplasmic FGFR2 expression in 26.7% of the normal tissues. Of the 125 breast cancer specimens, they found high cytoplasm expression in 81 (64.8%) samples. And high nuclear expression of FGFR2 was found in 6 of 30 (20%) benign tissues, compared with 71 of 125 (56.8%) breast cancer tissues [12]. In addition, Anita L *et al.* reported FGFR2 protein was more highly expressed in BRCA2-associated breast cancers [13]. Therefore, FGFRs, especially FGFR2, are potential therapeutic targets for tumor. A short peptide named 8B13 is mimic peptide of FGF-8b. The amino acid sequences of 8B13 is PNFTQHVREQLV. Peptide 8B13 can inhibit prostate carcinoma cells by means of antagonizing FGF-8b and then competitively binding FGFRs possibly[14]. In our study, we have utilized isothermal titration calorimetry (ITC) to prove that 8B13 has affinity with FGFR2.

Chitosan (CS) is one kind of common pharmaceutical excipients with many excellent physicochemical property, including biocompatibility, biodegradability, nontoxicity, etc. Chitosan were usually used to combine with various ligands, including folic acid, Arg-Gly-Asp peptide, hyaluronic acid, etc [15].

The purpose of this research is to prepare a photodynamic agent based on GQDs and peptide 8B13 for tumor PDT. In order to improve stability of fluorescence, GQDs were modified by polydopamine. Peptide 8B13 which combined chitosan via EDC/NHS reaction served as tumor targeting ligand. With the purpose of reducing phototoxicity during drug delivery, we utilized 8B13-coupled chitosan (CS-8B13) to coat PDA-GQDs via electrostatic attraction and adhesive ability of PDA. We designed that chitosan, a degradable materials, shelter GQDs from illumination during drug delivery. When PDA-GQDs/CS-8B13 arrives at tumor and then releases GQDs, PDT are carried out (Fig.1). In this study, PDA-GQDs/CS-8B13 was prepared. Physical characterization and pharmacodynamics in vitro of PDA-GQDs/CS-8B13 were studied.



Fig. 1 Schematic illustrating the preparation of PDA-GQDs/CS-8B13 nanohybrids and the nanohybrids targeting FGFR2.

2. Experiment Content

2.1 Material

GQDs were purchased from Qingdao Haida Haixi new materials Co. Ltd. Dopamine and dialysis membranes were obtained from Sigma-Aldrich, USA. Reactive oxygen species assay kit, EDC, NHS, methyl thiazolyl tetrazolium (MTT), Annexin V-FITC apoptosis assays kit were purchased from Shanghai beyotime Biological Technology Co. Ltd. Low molecular weight chitosan (~5 kDa) was

purchased from Zhejiang Golden Shell Pharmaceutical Co. Ltd. Peptide 8B13 was obtained from chinapeptides Co. Ltd.

2.2 Isothermal Titration Calorimetry

The affinity between peptide 8B13 and FGFR2 was measured by MicroCal iTC200. FGFR2 (3.2 μM) was equilibrated in reaction buffer at 25 $^{\circ}\text{C}$ in the sample cell and the reference cell was load with ultrapure water. The syringe cell was filled with 8B13 (100 μM). FGFR2 was titrated with 20 injections of 2 μL 8B13 and heat response was recorded (the volume of the first injection drop was 0.4 μL). The rotate speed was 750 R/min and system temperature was 25 $^{\circ}\text{C}$. Data were fitted with ORIGIN software.

2.3 Synthesis of 8B13 Coupled-Chitosan

Peptide 8B13 combined chitosan via amidation similar to those previous studies [16,17] Peptide 8B13, 60 mg, was first dissolved in 10 mL of PBS (pH6) followed adding 75 mg of EDC.HCl and 45 mg of NHS for stirring at 4 $^{\circ}\text{C}$ for 15 min. Chitosan, 100 mg, was dispersed in 10 mL of PBS (pH6). Then chitosan was dropwise added to the solution of Peptide 8B13. The final solution was stirred for 24 h at 4 $^{\circ}\text{C}$ in the dark. The final solution was dialyzed in ultrapure water with dialysis membrane (MW = 3.5 kDa). The dialyzed solution was then freeze-dried and stored at -20 $^{\circ}\text{C}$. The characteristic absorption bands related with functional groups of 8B13 and CS were detected by means of Fourier transform infrared (FTIR) spectroscopy.

2.4 Preparation of PDA-GQDs/CS-8B13

PDA-GQDs were prepared according to a reference with modification. Dopamine, 50 mg, was dissolved in 100 mL of Tris-HCl (1 M, pH8.5) and then stirred for 3 h. Forty milliliters of PDA were added to 40 mL of GQDs (1 mg/mL). The pH of the solution mixing PDA and GQDs was adjusted to 4.5. Then, the solution was stirred for overnight in the dark. PDA-GQDs suspension was dialyzed in ultrapure water with dialysis membrane (MW = 3.5 kDa). CS-8B13, 40 mg, was added to the PDA-GQDs suspension and then stirred for 24 h, at 4 C in the dark. PDA-GQDs/CS-8B13 suspension was dialyzed in ultrapure water with dialysis membrane (MW = 7 kDa). The final suspension was passed through a 0.45 μm syringe filter and then freeze-dried.

2.4 Chemical Characterization

PDA-GQDs/CS-8B13 freeze-dried powder was dispersed in ultrapure water. The zeta potential and particle size were characterized using malvern laser particle size analyzer. PDA-GQDs/CS-8B13 or GQDs were dropwise added to the mica sheets. After air-drying, the mica sheets were characterized using bioscope catylyst nanoscope-V which is one kind of atomic force microscope (AFM). PDA-GQDs/CS-8B13 was also characterized using transmission electron microscope (TEM). The loading ratio of GQDs (w/w%) was determined from fluorospectro photometer emission wavelength at 450 nm (excitation wavelength at 280 nm).

2.5 Cell Culture and Cellular Uptake of PDA-GQDs/CS-8B13

Human breast cancer SKBR-3 cells and MDA-MB-231 cells were purchased from Shanghai Institute of Cell Biology, Chinese Academy of Sciences. SKBR-3 cells were cultured in DMEM supplemented with 10% FBS at 37 $^{\circ}\text{C}$ under a 5% CO_2 humidified atmosphere. MDA-MB-231 cells were cultured in 1640 supplemented with 10% FBS and 5% horse serum at 37 $^{\circ}\text{C}$ under a 5% CO_2 humidified atmosphere. It has been reported that FGFR2 protein expression level of SKBR-3 is higher in comparison with MDA-MB-231. Moreover, compared with MDA-MB-231 cells, SKBR-3 cells also express more proteins of FGFR1 and FGFR3. SKBR-3 and MDA-MB-231 were respectively seeded in laser confocal culture dish. After incubation for overnight, the medium was replaced with fresh medium containing 100 $\mu\text{g}/\text{mL}$ of PDA-GQDs/CS-8B13. After incubation for 2 h, cells were fixed with 4% formaldehyde for 15 minutes and then incubated in 1% BSA for 1 h. The cells were incubated with the FGFR2 antibody (5 $\mu\text{g}/\text{ml}$) overnight at 4 $^{\circ}\text{C}$. The secondary antibody (Red) was Alexa Fluor 555-labeled Donkey Anti-Rabbit IgG (H+L) used at a 1/1000 dilution for 1h. Hoechst was used to

stain the cell nuclei (blue). The cells were imaged under a confocal laser fluorescence microscope (LSM 700, Zeiss).

2.6 PDT and Dark Toxicity in Vitro

Cell viability was measured by MTT assay. SKBR-3 cells and MDA-MB-231 cells were respectively cultured in 96 wells plate at a density of 8000 cells per well for 24 h. The cells were treated with different concentrations of PDA-GQDs/CS-8B13 or different concentrations of GQDs for 20 h. The serum-free medium was replaced with fresh serum-free medium with the purpose of removing free GQDs-PDA/CS-8B13 or free GQDs which did not get into cytoplasm. The cells were exposed to the illumination of LED light (425 ± 10 nm) for 20 min. And then the cells were incubated for 4 h. MTT solution (20 μ L) was added to each well, and the cells were incubated at 37 °C for 4 h again. The medium was replaced with DMOS. The absorbance was measured at 490 nm. The apoptosis induced by PDA-GQDs/CS-8B13 being exposed to illumination was also measured using flow cytometry.

2.7 ROS Production

SKBR-3 cells and MDA-MB-231 cells were cultured in 6 wells plate for 24 h. The cells were treated with different concentrations of PDA-GQDs/CS-8B13 for 20 h. The medium was replaced with fresh serum-free medium containing 10 μ M/L of DCFH-DA. In the meantime, this procedure removed the free GQDs-PDA/CS-8B13. The cells were incubated for 1 h and then exposed to illumination of LED light for 20 min. The cells were collected and washed with PBS three times. The ROS production was measure using flow cytometer and represented using Geo.mean of FL1.

2.8 Statistical Analysis

Values were expressed as means \pm standard deviations. Statistical analysis was performed using the Student's t test. Values of $p < 0.05$ were considered to be statistically significant.

3. Result and Discussion

3.1 Affinity between Peptide 8B13 and FGFRs

Peptide 8B13 is mimic peptide of FGF-8b which has ability to specifically bind FGFRs. We speculate that peptide 8B13 also has affinity with FGFRs. As a matter of fact, peptide 8B13 specifically binding FGFR2 was proved by means of ITC. The thermal power-time curve and heat-flux difference-molar ratio (ligand/receptor) fitted curve were presented in Fig. 2. The affinity constant (K_D) between peptide 8B13 and FGFR2 was 0.14 mM. Binding-site number (n) was 1.07×10^{-7} . Molar binding enthalpy (ΔH) and molar binding entropy (ΔS) respectively were 2.40×10^{10} kJ/mol and 8.04×10^7 kJ/mol. Previous study reported that the affinity constant (K_D) between peptide FGF-1 and FGFR2 was 4.3 μ M [18]. Therefore, compared with FGF-1, peptide 8B13 has stronger affinity with FGFR2. Besides, according to the thermal power-time curve, the procedure that peptide 8B13 combined FGFR2 absorbed heat first and then gave out heat, which indicated that there were two type of binding sites at least. Although, we cannot prove peptide 8B13 has ability to bind FGFR1, FGFR3 and FGFR4 for available data. Peptide 8B13 has ability to specifically bind FGFR2 at least.

3.2 Conjugation of Chitosan with 8B13

Peptide 8B13 combined chitosan via EDC/NHS reaction. The coupled reaction occurs at the carboxyl groups of peptide 8B13 and amino groups of chitosan. The FTIR spectrums of chitosan, peptide 8B13 and CS-8B13 were presented in Fig. 3. In the FTIR spectrum of chitosan, the broad peak at 3449 cm^{-1} was stretching vibration of N-H. The peak at 1598 cm^{-1} was in-plane bending vibration of $-\text{NH}_2$. In the FTIR spectrum of 8B13, the peak at 1629 cm^{-1} was stretching vibration of C=O. In the FTIR spectrum of CS-8B13, the peak at $\sim 1598 \text{ cm}^{-1}$ ($-\text{NH}_2$) for CS shifted to a higher wavelength at 1625 cm^{-1} for CS-8B13. This phenomenon indicated that lone pair electrons of nitrogen-atoms on chitosan p - π conjugated carbonyl group of 8B13 [19]. On the other hand, new peak at $\sim 1549 \text{ cm}^{-1}$ (in-plane bending vibration of amide linkage) appeared. These data draw a conclusion that peptide 8B13 conjugates chitosan successfully.

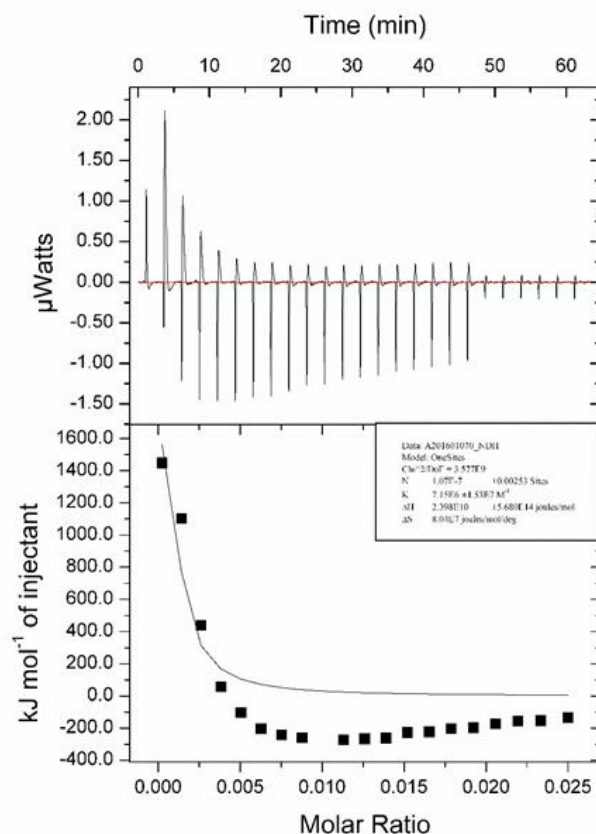


Fig. 2 ITC titrations of peptide 8B13 to FGFR2. FGFR2 (3.2 μM) was titrated with injections of 100 μM peptide 8B13. Data were fitted with ORIGIN software. The raw ITC data are shown in the top graph. The bottom graph was heat-flux difference-molar ratio (ligand/receptor) fitted curve.

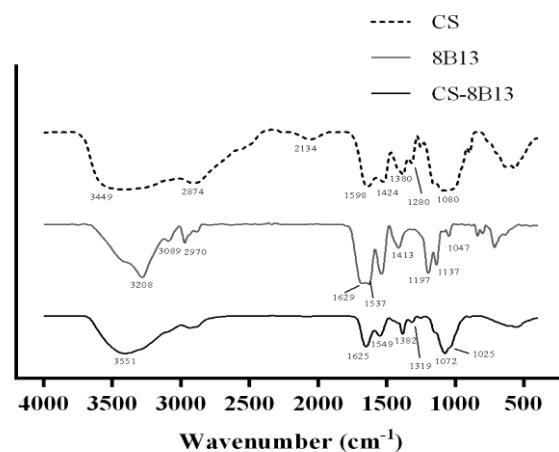


Fig. 3 Fourier transform infrared spectra of CS, 8B13 and CS-8B13.

3.3 Conjugation of Chitosan with 8B13

The GQDs emit blue-green fluorescence (Fig. 4A). It has been reported that PDA has adhesive force and improve fluorescence stability for GQDs [8]. It is possible that PDA improves GQDs fluorescence stability by means of inhibiting aggregation and protonation. On the other hand, for sake of reducing phototoxicity during drug delivery, PDA-GQDs/CS-8B13 was prepared.

The particle size and zeta potential of PDA-GQDs/CS-8B13 respectively were 219 ± 28 nm and 1.33 ± 1.54 mV (Fig. 4B). The zeta potential approximated zero due to the fact that the combination between PDA-GQDs (negative charge) and CS-8B13 (positive charge) by means of electrostatic

attraction and adhesive force. As show in Fig. 4C and Fig. 4D, the particle size of GQDs is 3 nm~25 nm, while the diameter of PDA-GQDs/CS-8B13 was ~150 nm. PDA-GQDs/CS-8B13 nanoparticles were obvious larger than GQDs. However, the thickness was only 15~25 nm. It kept the shape of spheroid (sheet). It is possible that CS-8B13 covered multi-PDA-GQDs. The adhesive force of PDA gave rise to aggregation among a few of PDA-GQDs. In addition, PDA-GQDs/CS-8B13 was rougher than GQDs owing to PDA and CS-8B13 (Table 1). As show in the TEM figure (Fig. 4E), the diameter of PDA-GQDs/CS-8B13 was also ~150 nm similar to the result of AFM. After phosphotungstic acid staining, PDA-GQDs/CS-8B13 presented positive staining result indicating that CS-8B13 covered PDA-GQDs successfully. Because the amidogen and hydroxyl of CS-8B13 interacted with phosphotungstic acid leading to positive staining result. The loading capacity of GQDs was found to be $51.78 \pm 8.26\%$ (w/w%) of the nanohybrids.

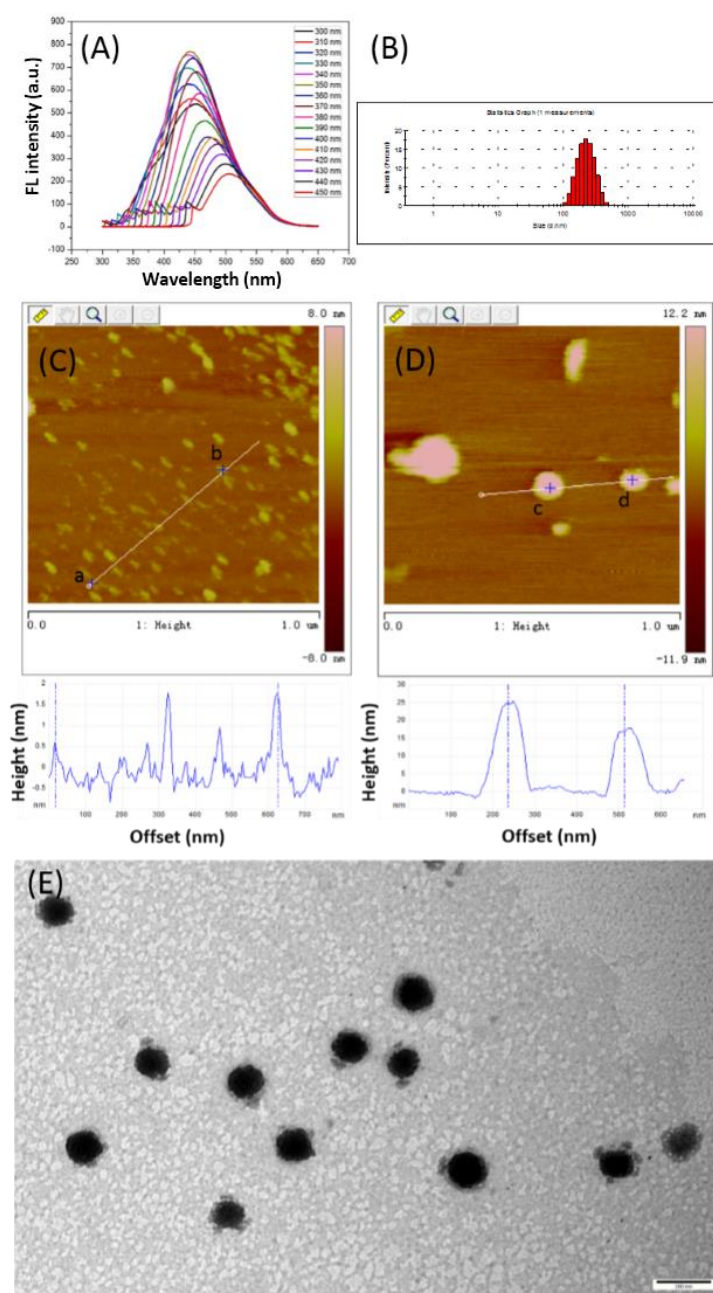


Fig. 4 The fluorescence emission spectrum of GQDs at different excitation wavelength (A). The particle size distribution of PDA-GQDs/CS-8B13 (B). AFM images of GQDs (C) and PDA-GQDs/CS-8B13 (D). The bottom graphs respectively represented the cross-section analysis for axis ab and axis cd. TEM image of PDA-GQDs/CS-8B13 (E).

Table 1 The cross-section analysis for axis ab and axis cd

axis	Horizontal Distance	Vertical Distance	Rmax	Rz	Rms	Ra (Frequency Cutoff)
ab	610.20 nm	1.19 nm	2.60 nm	1.064 nm	0.40 nm	0.32 nm
cd	279.71 nm	-7.54 nm	27.90 nm	27.90 nm	9.70 nm	6.97 nm

Note: Rmax, maximum vertical distance between the highest and lowest data points in the image following the plane fit. Rz, the average difference in height between the five highest peaks and five lowest valleys relative to the mean plane. Ra, arithmetic average of the absolute value of the surface height deviations measured from the mean plane. Rms, root-mean-square roughness.

3.4 Targeting Drug-Delivery System

In order to confirm whether PDA-GQDs/CS-8B13 could target FGFR2 in cellular environment, we used SKBR-3 and MDA-MB-231 as cell models. The FGFRs protein content of SKBR-3 cells, including FGFR2, was considerably more abundant in comparison with MDA-MB-231 cells [20,21]. The PDA-GQDs/CS-8B13 fluorescence and FGFR2 immunofluorescence were used to quantify and position. As show in Fig. 5, SKBR-3 exhibited considerably stronger green fluorescence (PDA-GQDs/CS-8B13) and stronger red fluorescence (FGFR2). The result demonstrated that cells took in PDA-GQDs/CS-8B13 within 2 h and the cellular uptake was mediated by FGFR2 at least. Because peptide 8B13 may bind with other FGFRs, green fluorescence (PDA-GQDs/CS-8B13) and red fluorescence (FGFR2) partially overlapped. Alternatively, GQDs have got rid of the nanohybrid.

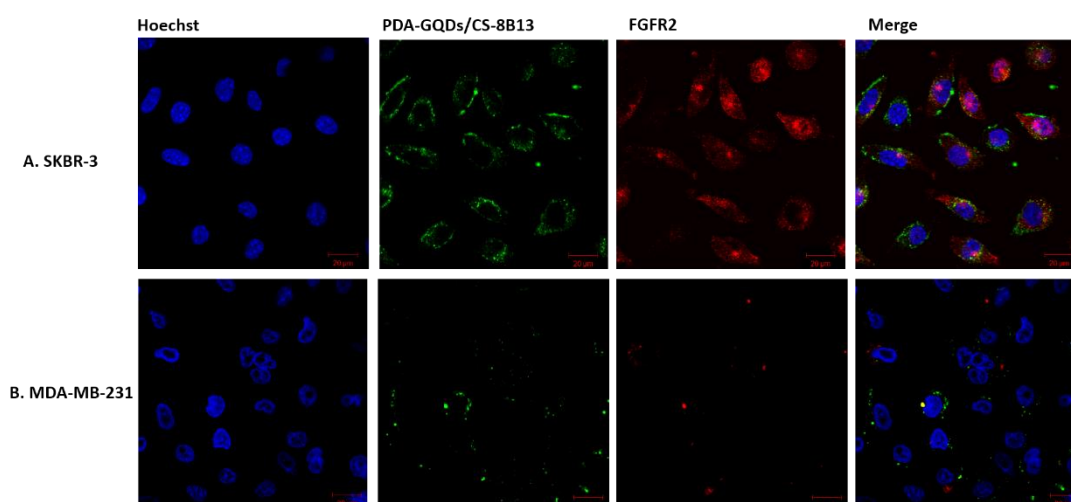


Fig. 5 Confocal microscopic images of SKBR cells and MDA-MB-231 cells incubated with PDA-GQDs/CS-8B13 (100 $\mu\text{g}/\text{mL}$) for 2 h. Left to right columns: hoechst stain images, PDA-GQDs/CS-8B13 fluorescence images, FGFR2 immunofluorescence images, overlay of the corresponding images.

3.5 PDT Assay

The in vitro phototoxicity and targeting efficiency of the nanoparticles for SKBR-3 cells and MDA-MB-231 cells in comparison with GQD alone was measured by MTT. On the other hand, in order to guarantee the safety of PDT agent, dark toxicity of PDA-GQDs/CS-8B13 was measured. As show in Fig. 6B, PDA-GQDs/CS-8B13 did not show cytotoxicity within the tested concentration range without illumination. Treated with GQDs or PDA-GQDs/CS-8B13 and illumination, the cell viabilities decreased with concentration increase. Compared with GQDs, PDA-GQDs/CS-8B13 inhibited more cells from surviving both SKBR-3 and MDA-MB-231 (Fig. 6A). In comparison with MDA-MB-231, PDA-GQDs/CS-8B13 inhibited more SKBR-3 cells from surviving (except the concentration of 10 $\mu\text{g}/\text{mL}$). Besides, 25 $\mu\text{g}/\text{mL}$ of GQDs approximated saturation concentration for both SKBR-3 cells and MDA-MB-231 cells, while 50 $\mu\text{g}/\text{mL}$ of PDA-GQDs/CS-8B13 approximated saturation concentration. The apoptosis result of flow cytometry was similar to MTT assay (Fig. 7).

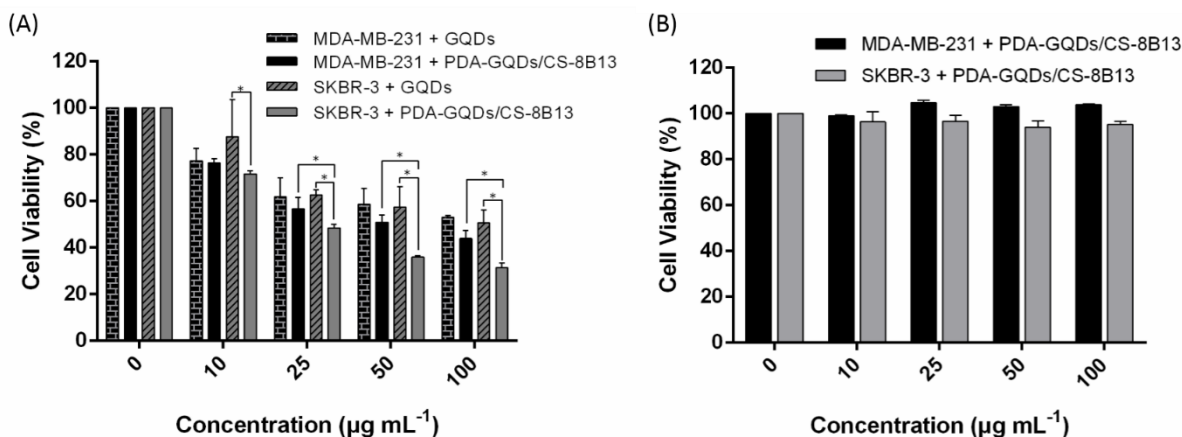


Fig. 6 Evaluation of the photo-activity of PDA-GQDs/CS-8B13 nanocomposites. (A) Cells treated with different concentration of PDA-GQDs/CS-8B13 or GQDs and exposed to illumination for 20 minutes. (B) Cells treated with different concentration of PDA-GQDs/CS-8B13 without illumination. Data are presented as the means \pm SD (n = 3), *P < 0.05.

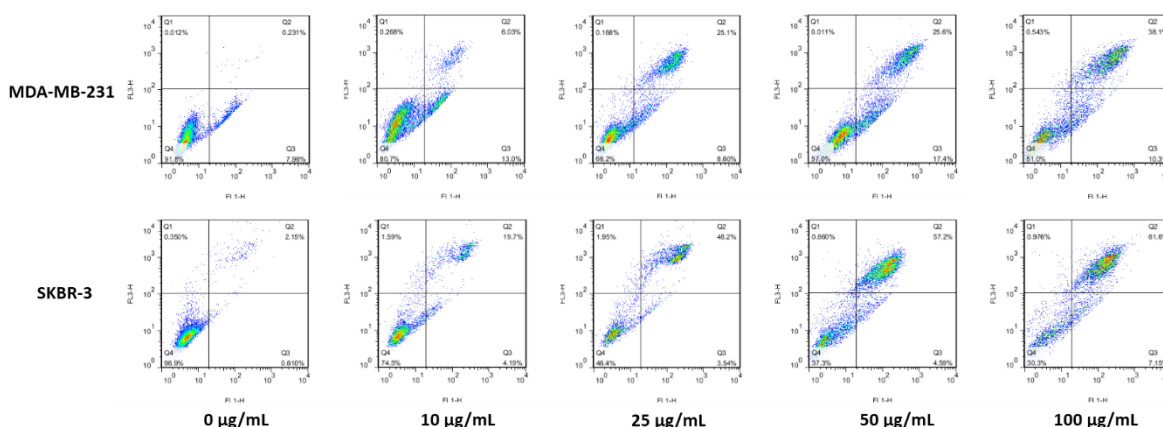


Fig. 7 Apoptosis were detected by FCM. SKBR-3 cells and MDA-MB-231 cells were incubated with different concentration of PDA-GQDs/CS-8B13 and exposed to illumination for 20 minutes.

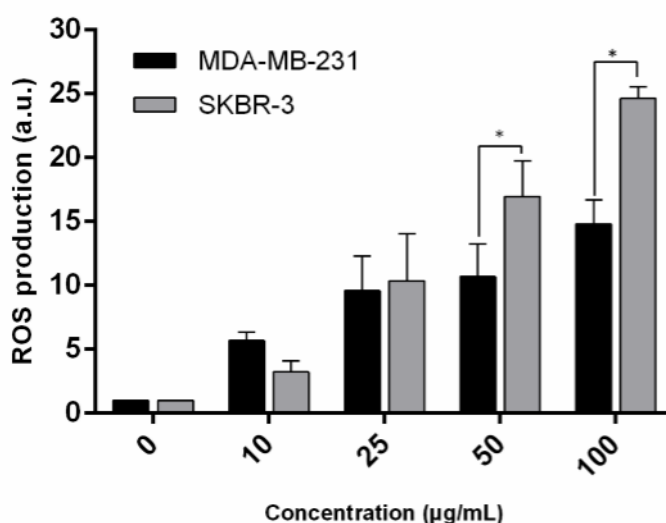


Fig. 8 Qualitative evaluation of ROS generated by PDA-GQDs/CS-8B13. SKBR-3 cells and MDA-MB-231 cells incubated with different concentration of PDA-GQDs/CS-8B13 and exposed to illumination for 20 minutes. The ROS production was measure using flow cytometer and represented using Geo.mean of FL1. Data are presented as the means \pm SEM (n = 3), *P < 0.05.

3.6 ROS Production

As shown in Fig. 8, ROS production increased with concentration of PDA-GQDs/CS-8B13. According to preceding part of the text, 50 µg/mL of PDA-GQDs/CS-8B13 approximated saturation concentration. However, the ROS productions between 50 µg/mL and 100 µg/mL has significant difference. It was possible that low-concentration PDA-GQDs/CS-8B13 has already triggered autophagy inducing apoptosis.

4. Conclusion

In summary, peptide 8B13-coupled chitosan covered PDA-modified GQDs were prepared for PDT. PDA-GQDs/CS-8B13 whose particle size was about 200 nm took the shape of spheroid (sheet). SKBR-3 cells and MDA-MB-231 cell were used to make comparison for the nanoparticles targeting FGFR2. We found that PDA-GQDs/CS-8B13 preferred targeting SKBR-3 with high FGFR2 expression rather than MDA-MB-231 with low FGFR2 expression. The nanohybrid exhibited hypotoxicity without illumination, while they showed strong phototoxicity after illumination. They damaged cells by means of producing ROS. Although, these data may raise possibility of PDA-GQDs/CS-8B13 as potential agent for breast tumor PDT in vitro. Further studies are necessary to study them in vivo.

Acknowledgements

This work was supported in part by National Natural Science Foundation of China(81202454), the Guangdong Province Higher Vocational Colleges and Schools Pearl River Scholar Funded Scheme (2012) and Project of Research Development and Industrialization of Guangdong Province (2013B090500046) .

References

- [1] Zheng XT, Ananthanarayanan A, Luo KQ and Chen P: Glowing graphene quantum dots and carbon dots: properties, syntheses, and biological applications, *Small*, Vol. 11 (2015) No. 14, p.1620.
- [2] Nurunnabi M, Parvez K, Nafiujjaman M, Revuri V, Khan HA, Feng X, et al. Bioapplication of graphene oxide derivatives: drug/gene delivery, imaging, polymeric modification, toxicology, therapeutics and challenges, *Rsc Advances*, Vol. 5 (2015) NO. 52, p.42141-61.
- [3] Wang X, Cao L, Lu F, Meziani MJ, Li H, Qi G, et al. Photoinduced electron transfers with carbon dots, *Chemical Communications*, Vol. 46 (2009) No. 25, p.3774-6.
- [4] Wu C, Wang C, Han T, Zhou X, Guo S, Zhang J: Insight into the cellular internalization and cytotoxicity of graphene quantum dots, *Advanced Healthcare Materials*, Vol. 2 (2013) No. 12, p.1613–9.
- [5] Jr JJR, Agostinis P, Berg K, Oleinick NL, Kessel D: Assessing autophagy in the context of photodynamic therapy, *Autophagy*, Vol. 6 (2010) No. 1, p.7-18.
- [6] Fimia GM, Piacentini M: Regulation of autophagy in mammals and its interplay with apoptosis, *Cellular & Molecular Life Sciences Cmls*, Vol. 67 (2010) No. 10, p.1581-8.
- [7] Kang X, Cai W, Zhang S, Cui S: Revealing the formation mechanism of insoluble polydopamine by using a simplified model system, *Polymer Chemistry*, Vol. 8 (2016).
- [8] Nurunnabi M, Khatun Z, Nafiujjaman M, Lee DG, Lee YK: Surface Coating of Graphene Quantum Dots Using Mussel-Inspired Polydopamine for Biomedical Optical Imaging, *Acs Applied Materials & Interfaces*, Vol. 5 (2013) No. 16, p.8246-53.
- [9] Katoh Y, Katoh M: FGFR2-related pathogenesis and FGFR2-targeted therapeutics (Review), *International Journal of Molecular Medicine*, Vol. 23 (2009) No. 3, p.307.
- [10] André F, Cortés J: Rationale for targeting fibroblast growth factor receptor signaling in breast cancer, *Breast Cancer Research and Treatment*, Vol. 150 (2015) No. 1, p.1-8.

- [11] Tenhagen M, van Diest PJ, Ivanova IA, Van dWE, Van dGP: Fibroblast growth factor receptors in breast cancer: expression, downstream effects, and possible drug targets, *Endocrine-related cancer*, Vol. 19 (2012) No. 4, p.R115.
- [12] Shanshan Sun MD, Yongdong Jiang MD, Guoqiang Zhang MD, Song H, Xianyu Zhang MD, Zhang Y, et al. Increased expression of fibroblastic growth factor receptor 2 is correlated with poor prognosis in patients with breast cancer, *Journal of Surgical Oncology*, Vol 105 (2012) No. 8, p.773.
- [13] Bane AL, Colby PS: Expression profiling of familial breast cancers demonstrates higher expression of FGFR2 in BRCA2 -associated tumors, *Breast Cancer Research and Treatment*, Vol. 117 (2011) No. 1, p.183-91.
- [14] Li T, Luo W, He D, Wang R, Huang Y, Zeng X, et al. A short peptide derived from the gN helix domain of FGF8b suppresses the growth of human prostate cancer cells, *Cancer Letters*, Vol.339 (2013) No. 2, p.226-36.
- [15] Ghaz-Jahanian MA, Abbaspour-Aghdam F: Application of Chitosan-Based Nanocarriers in Tumor-Targeted Drug Delivery, *Molecular Biotechnology*, Vol. 57 (2015) No. 3, p.201-18.
- [16] Reis LA, Chiu LL, Liang Y, Hyunh K, Momen A, Radisic M: A peptide-modified chitosan-collagen hydrogel for cardiac cell culture and delivery, *Acta Biomaterialia*, Vol. 8 (2012) No. 3, p.1022-36.
- [17] Rask F, Dallabrida SM, Ismail NS, Amoozgar Z, Yeo Y, Rupnick MA, et al. Photocrosslinkable chitosan modified with angiopoietin-1 peptide, QHREDGS, promotes survival of neonatal rat heart cells, *Journal of Biomedical Materials Research Part A*, Vol. 95 (2010) No. 1, p.105-17.
- [18] Brown A, Robinson CJ, Gallagher JT, Blundell TL: Cooperative Heparin-Mediated Oligomerization of Fibroblast Growth Factor-1 (FGF1) Precedes Recruitment of FGFR2 to Ternary Complexes, *Biophysical Journal*, Vol. 104 (2013) No. 8, p.1720-30.
- [19] Hameka HF, Liquori AM: Some considerations on the dipole moments of azines, *Molecular Physics*, Vol.1 (1958) No. 1, p.9-13.
- [20] Czaplinska D, Turczyk L, Grudowska A, Mieszkowska M, Lipinska AD, Skladanowski AC, et al. Phosphorylation of RSK2 at Tyr529 by FGFR2-p38 enhances human mammary epithelial cells migration, *Biochimica Et Biophysica Acta*, Vol. 1843 (2014) No. 11, p.2461.
- [21] Zhu X, Asa SL, Ezzat S: Histone-acetylated control of fibroblast growth factor receptor 2 intron 2 polymorphisms and isoform splicing in breast cancer, *Molecular Endocrinology*, Vol. 23 (2009) No. 9, p.1397-405.